MATERIALS & METHODS

2.1 Description of the Study area

2.1.1 Location & background information

The study area, Shoolpaneshwar wildlife sanctuary (SWS), surveyed during the present research is situated in the hilly ranges of Narmada district in South Gujarat, INDIA (Figure 1). The SWS is an extension of old Dumkhal sloth Bear sanctuary falling in Dediapada and Nandod taluka of Narmada district. It is spread over five territorial ranges under the administrative control of Rajpipla East Division. The forest ranges are Piplod, Sagai, Fulsar, Gora and Dediapada which covers an area of 675 sq. km. Latitude and longitude of the study area is 21^0 29'N - 21^0 52'N and 73^0 29'E - 73^0 54'E respectively.

2.1.2 Physiography & Drainage

The sanctuary forms a connecting link between Vindhyan and Satpura ranges. The area has a rolling topography characterized by high degree of ruggedness and erosion. The hilly terrain with precipitous slopes at most of the places is a characteristic feature of the area. The hills vary in height between 400m-882m above msl. Dhaman mal hill near Waghumar village in Piplod range is the highest point in the sanctuary at 880.87m. Slopes, in general, are moderate to steep with general slope of the area being towards west.

The area is bounded in the North by the Sardar Sarovar and Narmada River and in the west by Karjan River, Karjan Reservoir and Tarav River. Most of the Eastern Boundary runs along 'Devganga River'. Thus, the sanctuary is surrounded by water sources on three sides. A large number of small rivulets and stream originate from the network of hillocks in the area and finally form the tributaries of Tarav, Karjan and Narmada rivers. The entire SWS is well drained by large number of streams and rivulets during monsoon (July – October). In summer (March – June) many of these streams are getting dried and flow of water ceases. At some places water remains stored in small pools on the Rocky River beds.

.

37

2.1.3 Climatic conditions

Atmospheric and meteorological influences, principally moisture, temperature, wind, atmospheric pressure and evaporation of a region collectively form the climate of a region (Shukla & Chandel, 1989). The climate of the sanctuary is periodical with three well defined seasons viz., winter (November to February), summer (March to June) and Monsoon (June to September). The month of October acts as a transition period between monsoon and winter season. The failure in any one of these season critically affects the overall vegetation of the region very much.

In the month of March, temperature starts rising and the onset of summer season is indicated by leaf fall and almost simultaneously appearance of new leaves in many trees. April and May are the hottest months of the year and the maximum temperature rises up to $40^{0}C$. During winter season the temperature goes down and minimum temperature varies between $8^{0}C$ to $12^{0}C$. January is the coldest month. The fall in temperature during winter season and the rise in temperature during summer season are not uniform. Most of the time high temperatures prevail up to 2nd week of June. The summers are hot while the winters are pleasant.

The rainy season usually starts in June and lasts upto September. The maximum rainfall occurs during the month of July. High shower continue up to the 2nd week of October. The area receives an annual rainfall of 100 to 125cms. Relative humidity is the highest during the months of July and August (81-93%). It decreases to its minimum during winter (30-40%).

2.1.4 Geology & Soil

The sanctuary falls within the lower Narmada valley which geologically includes the Precambrian basement metamorphics and granites, cretaceous Baghbeds and their fresh water equivalents, Deccan trap and associated intrusive, Tertiary sedimentary deposits and quaternary alluvium (Deota, 1991). The Deccan trap is the main geological formation encountered in the lower Narmada valley. The major geological formations met within the study area in sequence of deposition are Bagh limestone, sand stones, the deccan trap lava flows and the alluvial deposits.

38

stoniness depending upon the rock and topography. The reddish brown loamy soil, yellowish brown loamy soil, sandy loam, fine murram and black cotton soil are some of the soils found in the sanctuary area. Reddish brown loam, found on gentle slopes, hilltops and undulating plains, is formed by the disintegration of trap rocks. Clayey loam and black clay are the latest alluvial deposits, representing rich and deep soils. Such soils are mostly found in flat portions and form excellent forest soil supporting good forests and ample natural regeneration.
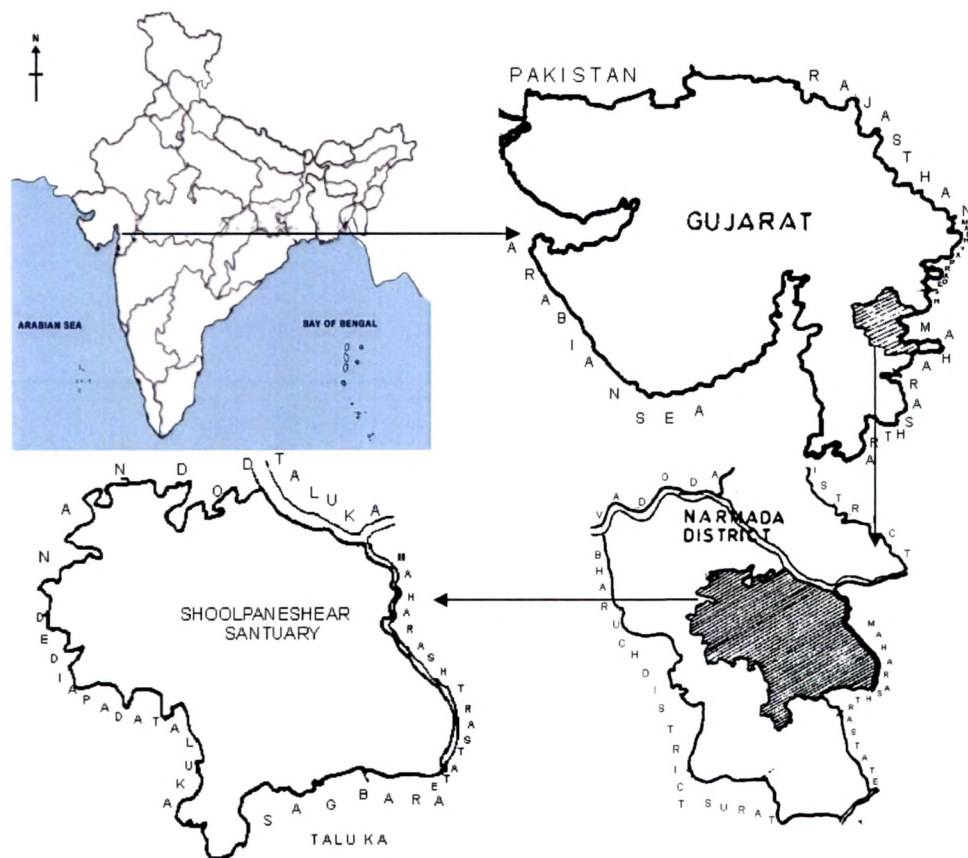

Figure 1: Location map of the Shoolpaneshwar Wildlife Sanctuary

2.1.5   Major types of Forests

The forest vegetation prevailing in the sanctuary can be broadly grouped into,

    1.5.1. Moist, mixed deciduous forest

    1.5.2. Dry, mixed deciduous forest.

    1.5.3. Riverain forest

2.1.5.1. Moist, mixed deciduous forest

As per the Champion & Seth's "Classification of forest types" this group belongs to the type of "Southern Tropical Moist Deciduous Forest". This generally is confined to the valleys and plains having good soil moisture. Trees have almost closed canopy and the leafless period begins by the end of the cold season. These areas support good varieties of plant species (Figure 2). The floristic composition mainly includes tree species viz: *Terminalia crenulata* Roth (Sadad), *Adina cordifolia* Salisb. (Haldarvo), *Tectona grandis* L. (Sag), *Mitragyna parviflora* Korth. (Kalam), *Dalbergia latifolia* Roxb. (Sisam), *Anogeissus latifolia* Wall. (Dhavado), *Bridelia retusa* Linn. (Asan), *Albizia lebbeck* Linn. (Siris). –Middle storey is occupied by *Butea monosperma* Lamk. (Palas), *Holarrhena antidysenterica* R. Br. (Indra-jav), *Meyna laxiflora* Link. (adsu) and *Bauhinia racemosa* Lamk. (Asintro). The under storey mainly consists of small shrubs, under shrubs and herbs including grasses. It is represented by *Azanza lampas* Cav. (Jangli Paras), *Helicteris isora* Linn. (Antedi), *Eranthemum roseum* Vahli. *(*Dashmuli*)*. The ground cover mainly consists of herbs *like Sida cordata* Burm. F. *(*Bal*)*, *Neuracanthus sphaerostachys* Dalz., *Haplanthus verticillatus* Nees. *and Achyranthes aspera* L., etc. This ground cover and under storey is more prominent during monsoon. *Ventilago denticulate* Willd. (Asaivel), *Combretum ovalifolium* Roxb. *(*Dhummas*)*, *Phanera integrifolia* Roxb., *Cocculus hirsutus* Linn. (Vasan) and *Abrus precatorius* Linn. (Chanothi) are the major climbers.

During monsoon and post monsoon periods the ground cover as well as the understorey show profuse growth and it lasts till the beginning of the summer season. During monsoon season because of the appearance of a number of ephemerals and a large number of short lived annuals the area appears very thick and looks as if it is a semievergreen to evergreen type of forest.

40

Figure 2: Photographs showing moist deciduous nature of the sanctuary

2.1.5.2. Dry mixed deciduous forest

As per the Champion & Seth's "Classification of forest types" this group belongs to the type of "Southern Tropical Dry Deciduous Forest". It is the major type of forest vegetation in Gujarat and has two distinct sub types a) Dry teak forest & b) Dry non-teak forest. Forest vegetation in SWS falls under the dry deciduous with teak as a dominant species. It is commonly found in areas with lesser availability of water and heavy biotic pressure (Figure 3). Floristics includes trees such as *Tectona grandis* L. (Sag), *Dendrocalamus strictus* Nees. (Bamboo), *Anogeissus latifolia* Wall. (Dhavado), *Garuga pinnata* Roxb. (Kakad), *Lannea coromendalica* Houtt. (Modad), *Mitragyna parvifolia* Korth. (Kalam), *Madhuca indica* Gmel. *(*Mahudo*)*, and *Pterocarpus marsupium* Linn. *(*Biyo*)*. The middle storey consists of *Butea monosperma* Lamk. (Palas), *Meyna laxiflora* Link. (adsu), *Holarrhena antidysentrica* R. Br. (Indra-jav) and *Aegel marmelos* Corr. (Billi). The understorey consists of *Helicteris isora* Linn. (Antedi), *Nyctanthus arbortristis* Linn. (Parijatak) and *kirganelia reticulate* Poir. (Shilavi). The ground cover is occupied by *Sida cordata* Burm. F. *(*Bal*)*, *Borreria stricta* L.F., *Haplanthus verticillatus* Nees., etc. Climbers mainly include *Combretum ovelifolium* Roxb. *(*Dhummas*)*,-*Ventilago denticulate* Wild. and *Abrus precatorius* Willd. (Asaivel). A few epiphytes and parasites such as *Vanda tessellate* (Roxb., *Dendrophthoe falcate Ett.*, *Viscum articulatum* Heyne. and *Cuscuta reflexa* Roxb., are commonly met with. During monsoon and post monsoon period the undergrowth become more prominent and the entire area of the sanctuary gives the impression of a semi-evergreen type of forest (Sabnis and Amin, 1992).

The dry deciduous nature of the forest, the species composition (teak and Bamboo as main species), the high temperatures, windy climate and drying effects make the area very vulnerable to wild fires in the month of February and extends throughout the summer from April to mid May.
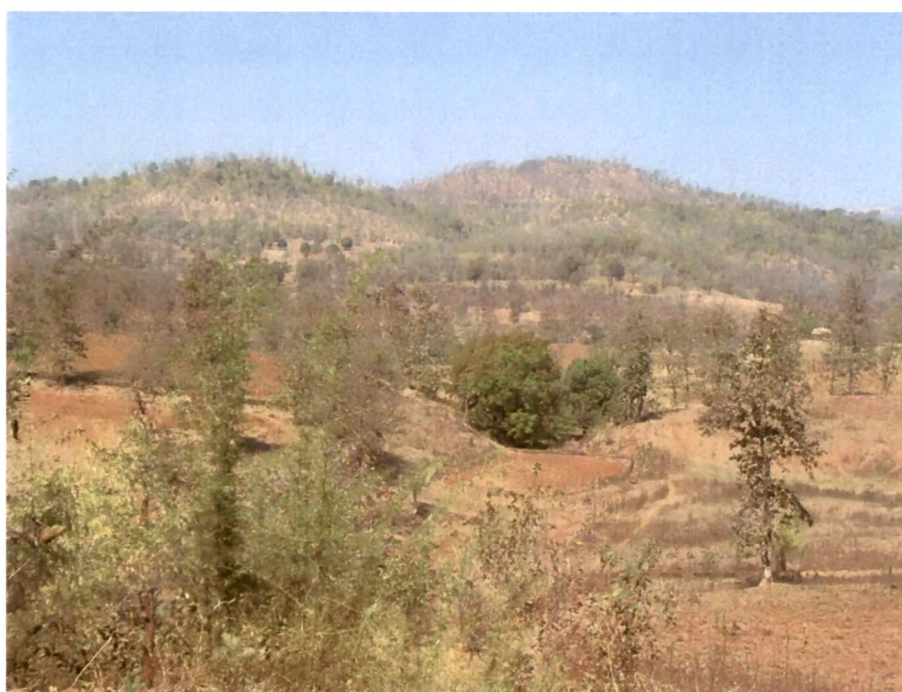
Figure 3: Photographs showing dry deciduous nature of the sanctuary

2.1.5.3. Riverain Vegetation

A number of streams and rivulets are present in the area. The herbivorous and other animals move towards the riverain areas during peak hours of heat for quenching their thirst and to take rest. The banks of rivulets and streams support luxuriant vegetation. Riverain vegetation is important as it supports the life of a large number of animal species during the peak summer months by providing green leaves to animals. The riverain vegetation in the area shows clear-cut zonations i.e. the banks especially the slopes support the growth of a large number of tree species, the region which is near to the water body and sometimes the exposed river beds as well as the fringes of streams support the growth of a number of herbs as well as grass species (Figure 4). Different species found on the banks and slopes are *Pongamia pinnata* Linn. (Karanj), *Ficus racemosa* Linn. (Umardo), *F. hispida* Linn. (Dhed umardo), *Vitex negundo* Linn. (Nagod), *Syzygium cumini* Linn. (Jambu) and *Dendrocalamus strictus* Linn. (Bamboo). On the river bed plants such as *Tamarix ericoides* Rottil. (Chhini), *Homonoia riparia* Lour. and *Polygonum glabrum* Willd. (Bosi) are generally present.

In addition there are plantations of *Tectona*, *Dendrocalamus* (Figure 5) and *Nyctanthus* in forest areas as well as along road sides carried out by forest department. Shoolpaneshwar Sanctuary, with its moist mixed deciduous forest and dry mixed deciduous forests provides a rich and conducive environment for animal and plant life. Different vegetation strata of trees, shrubs and herbs by providing variety of niches, support tremendous floral and faunal diversity which is comprising of 300 medicinal plants species, 21 mammals species, over 200 species of birds and 16 species of reptiles, large number of insects, fishes and invertebrate species. The Sanctuary has about 600 plant species belonging to Fungi group (18 sp.), bryophytes (6 sp.), pteridophytes (5 sp.) and angiosperms (571 sp.) including rare species (Saksena and Tyagi, 2002).

Figure 4: Photographs showing Riverine vegetation of the sanctuary

Figure 5: Photographs showing plantation of *Tectona grandis* L. and *Dendrocalamus strictus* Nees . in the sanctuary

46

2.1.6 Landuse pattern and biotic pressure

Larger part of the area is rugged and hilly to gently sloping terrain. North – west side of the sanctuary is mainly characterized by the presence of dense forest, steep hillocks and very less to negligible biotic pressure. Some of the areas can be seen with good forest patches on medium to gentle slopes. Northern side of the sanctuary is mainly characterized by submerged areas due to Sardar Sarovar Dam. Peripheral areas of the sanctuary is characterized by the presence of dry deciduous mixed type of forest vegetation where medium to severe biotic pressure, vast areas of agriculture field and heavy cattle grazing can be seen. Some of the localities show the deterioration of forest vegetation and the presence of agricultural land mostly in and around human inhabitation and along road side. Roads (193 km) are laid across the sanctuary for the movement of locals.

South – East portion of the sanctuary is completely denuded from vegetation (Figure 7). Areas such as Malsamot, Budi, Sakva, Bhilvasi, Surpan and Umarva represent severely deteriorated systems where the natural vegetation cover is replaced by agricultural crops and common weeds. SWS is inhabited by a large tribal population, which is spread across the sanctuary. The sanctuary has 105 villages inside and on the periphery. The peripheral area of the sanctuary is under high biotic pressure. Use of primitive agriculture practices like shifting cultivation has resulted in poor agriculture production, which has prompted people to bring more area under tillage. This resulted in encroachment of forest land. This lead to the shrinkage of habitat and some plant species show restricted distribution. Some scattered trees of *Madhuca indica* and *Mangifera Indica* are seen growing in this area. Tree species such as *Mangifera indica* and *Madhuca indica* are often planted by local tribals around their huts and agricultural fields (Figure 7).

The other categories of land i.e. private, revenue and *gaucher* – are largely used for agriculture. As far as revenue lands are concerned, they are largely used as grazing grounds. Landuse pattern can be easily discernable from the below given pie chart (Figure 6). The tribals inhabiting the sanctuary have the maximum interface with forest resources, it being the source for their survival and sustenance against the background of limited development opportunities. For vast spectrum of things the tribal depend heavily in this resource - timber for house construction, bamboo for house and fence repairs, grazing needs, non-timber forest products for bonafide use and for sale, collection and selling of seeds and making and selling of bamboo articles. Increasing population,

47

traditional attachment with land, poor literacy level, non development of technical skills, etc. are the factors that are increasing the dependence on forest resource. Besides the human population numbering over 36,000, the sanctuary also supports a cattle population double the human population (Saksena and Tyagi, 2002).
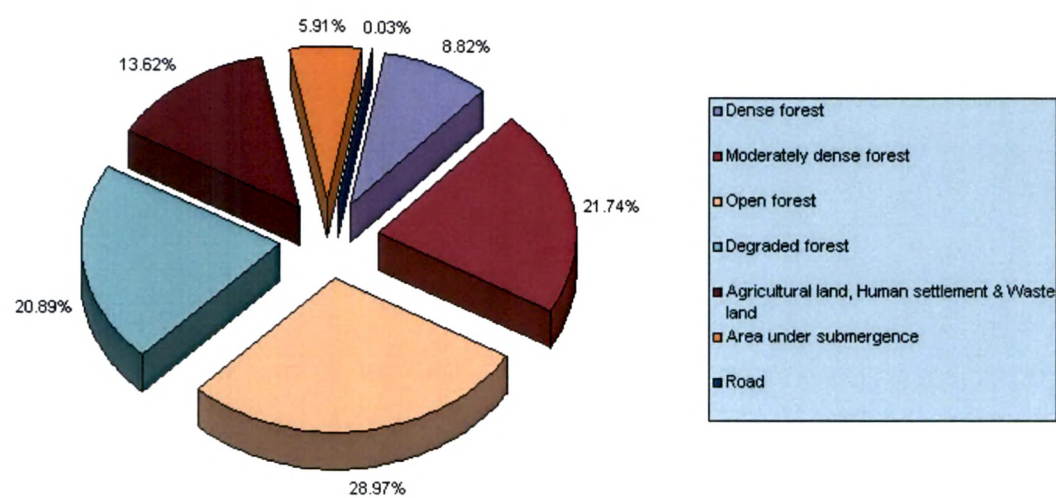

Figure 6: Pie Chart showing land use pattern across the sanctuary

(a)

(b)

Figure 7: (a) Photograph showing uncovered South-East area of the sanctuary, (b) photograph of Mangifera often planted by tribal near their hut

49

2.2 Data acquisition

2.2.1. Site & time selection for satellite path

Satellite path (Figure 8) was selected to cover maximum area of the sanctuary with distinct features. Center point of the satellite path is 21^0 42' 06" N latitude & 73^0 44' 06" E longitude which falls under Piplod range. This path represents the maximum vegetal cover with different levels of human disturbance compared to other areas of the sanctuary. Many water streams are also passing from this area which allows nearby vegetation to remain moist & green during summer. Plantation for *Tectona grandis* (Teak) and *Dendrocalamus strictus* (Bamboo) is available with 5-8 hectares spread. Furthermore, this selected path shows distinct permanent features like Sardar Sarovar dam, Tarav River, identifiable bridges for geometric correction.
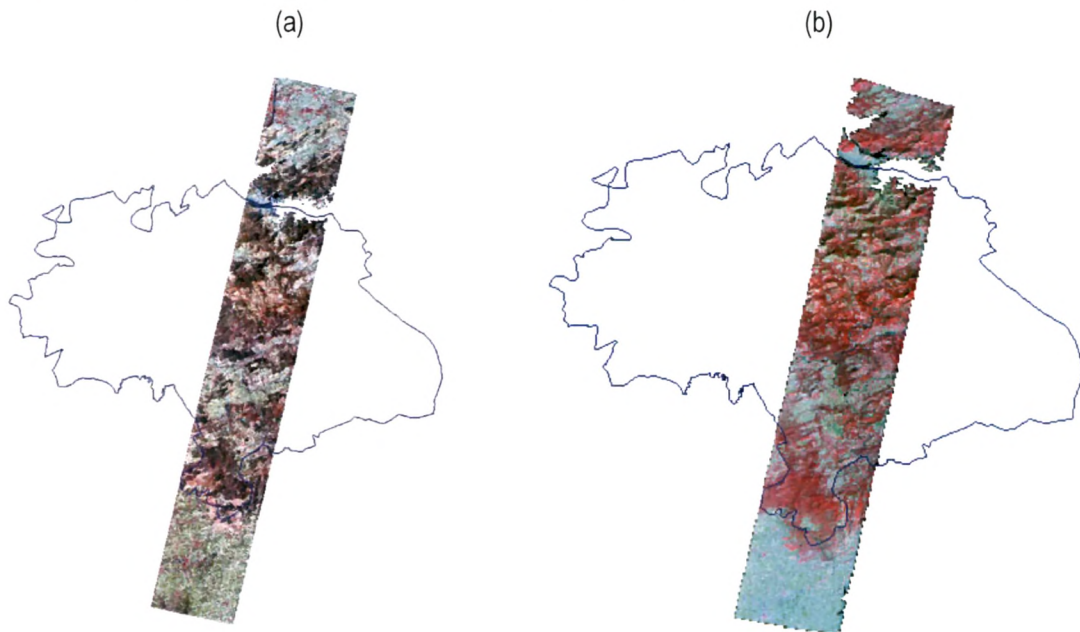
(a)   (b)

Figure 8: Satellite path across the study area in two different seasons (a) April (b) October

On April 03, 2006 and on October 21, 2006, EO-1 (USGS, USA) collected hyperspectral data in a 7.7km by 42km swath centered over the study area at nadir view (Figure 9). These dates were selected to demarcate the vegetation by phenology. Selected dates reflect seasonal variability in

the data sets. At the time of the satellite flight, the study area was showing < 25% cloud cover. In the month of April (dry season), vegetation was in different stages of senescence whereas in the month of October (wet season), vegetation was lush green due to seasonal change. Summer/Dry month (April) imagery is also useful to discriminate dry deciduous forest floor cover where litter acts as a load factor for forest fire.
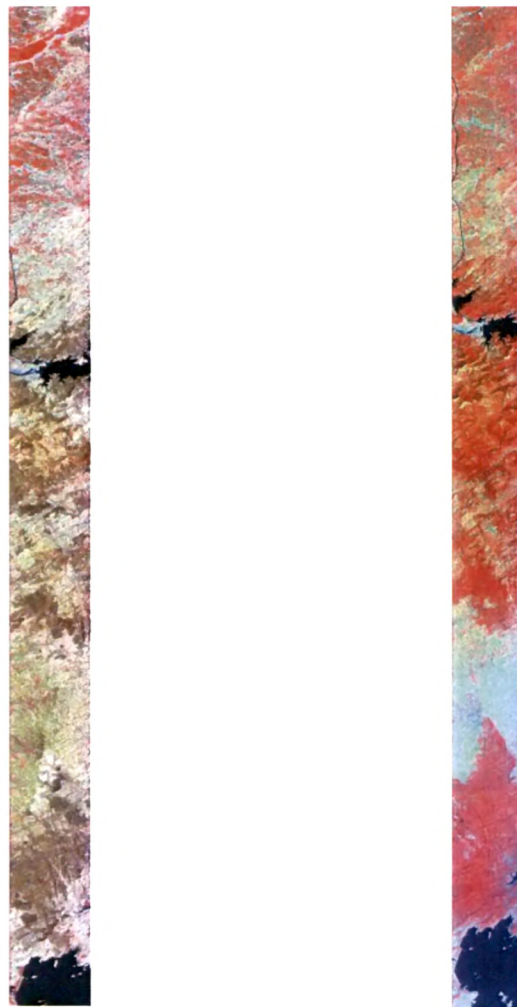

Figure 9: EO-I Hyperion satellite path of Shoolpaneshwar Wildlife Sanctuary from two different dates (a) 3rd April, 06 and (b) 21st October, 06.

2.2.2 Species selection

A preliminary survey was undertaken across the satellite path of the study area. The study area has a total of 127 tree species. Selection of study species was done based on purity (% area occupancy) and density. This helped to focus present study on 7 tree species for which there were sufficient recordable individuals on ground. Selected 7 tree species attributes are given in Table 1. The tree species represented both deciduous and evergreen types. The species chosen are very important for forestry operations in the SWS, Gujarat. *Tectona* and *Dendrocalamus* have high economic value in these parts of the world as they are significant contributors to timber sales. Other selected trees are used by locals to get NTFP (Non Timber Forest Products).

Table 1: Phenological attributes for selected tropical tree species (adapted from Cooke, 1967 and personal observations)

Tree species (family)	Leaf phenology functional group	Leaf exchange timing	3rd April leaf cover	21st October leaf cover
Tectona grandis Linn (Verbenaceae)	Deciduous	Annual	Low	High
Dendrocalamus strictus Nees (Poaceae)	Deciduous	Annual	Low	High
Mangifera indica Linn. (Anacardiaceae)	Evergreen	Continuous	High	High
Madhuca indica Gmel. (Sapotaceae)	Deciduous	Annual	Low	High
Ficus glomerata Roxb. (Moraceae)	Evergreen	Continuous	High	High
Pongamia pinnata Linn. (Leguminosae)	Evergeen	Continuous	High	High
Wrightia tinctoria R.Br. (Apocynaceae)	Deciduous	Annual	Low	High

2.2.3. Sensor characteristics

The National aeronautics and Space Administration (NASA), New Millennium Program (NMP) was created to flight-validated instrument and spacecraft technologies that may enable new or more cost-effective approaches to earth observation (Ungar et al., 2003). Both advanced multispectral and hyperspectral images were part of the NMP Earth Observing-1 (EO-1) mission. The Hyperion instrument (Figure 10) was built by TRW, Inc. (now Northrop Grumman Space Technology) with strong support from key sensor subsystem organizations.

The technology focus of EO-1 is the validation of sensors using "pushbroom" operation for space-based missions. There are two primary instruments on EO-1. The first, the Advanced Land Imager (ALI), is a ten-band multispectral system with multiple linear arrays embedded in a single sensor chip assembly (SCA). The other instrument, Hyperion, is a hyperspectral imager with 242 spectral channels, each 10 nm wide, spaced at 10-nm intervals across the spectral range from 400–2500 nm. The Hyperion pushbroom instrument was designed as a technology demonstration and provided high-quality calibrated data for hyperspectral application evaluations (Pearlman et al., 2003). Hyperion orbits the earth at 705km above mean sea level and one minute behind landsat. The Hyperion imaging slit is oriented perpendicular to the satellite's motion. The forward motion of the satellite creates a sequence of frames that were combined into a 2-D spatial image with a third dimension of spectral information (called a "three-dimensional data cube"). Each pushbroom image frame of Hyperion captures the spectra from an area 30 m along-track by 7.7 km cross-track (Figure 11) (Pearlman et al., 2003). The 7.7-km swath of Hyperion overlaps with the western 6 km of the 37-km swath of ALI (IEEE, 2003). Additional sensor characteristics of Hyperion are given in Tables 2 & 3.

2.2.4. Spectral Characteristics

The delivered USGS Hyperion product contains 242 bands, out of which 44 bands are not calibrated. The main reason for not calibrating all bands is due to decreased sensitivity of the detectors within the non-calibrated spectral regions. Out of the 242 collected bands, bands 1-7 (356 to 417 nm) and bands 225-242 (2406 to 2578 nm) are not calibrated. Bands 58-70 (collected by the VNIR instrument) and bands 71-76 (collected by the SWIR instrument) are also not calibrated. So, calibrated bands are 8-57 for VNIR, and 77-224 for the SWIR. Here, SWIR spectrum is divided into SWIR-1 (1300-1900nm) and SWIR-2 (1900-2500nm). Thus, the final L1R data product provides a total of 198 bands representing continuous spectra from 427 to 2395 nm. The collected and calibrated channels will also include a small area of spectral overlap between the VNIR and SWIR spectrometers (band 56 (915.23nm), band 57(925.41nm) and band 77(912.45nm), band 78(922.54nm) focal planes) (USGS, 2004). In the experiment, band 77 and 78 also were removed before further processing. Therefore final data contains 196 unique spectral channels. All bands that are not calibrated are set to zero (null values) in the Level 1R product.

Table 2: Characteristics of the Hyperion System (Pearlman et al., 2003)

Parameter	Hyperion
Volume (L x W x H, cm)	75 x 39 x 65
Weight (Kg)	49
Average Power (W)	51
Aperture (cm)	12
IFOV (mrad)	0.043
Crosstrack FOV (deg)	0.63
Wavelength Range (nm)	400-2500
Spectral Resolution (nm)	10
Number of Spectral Bands	242
Digitization (bits)	12
Frame Rate (Hz)	223.4

Table 3: Performance of the Hyperion instrument (Pearlman et al., 2003)

	Characteristic	On-orbit
OPTICAL	GSD (m)	30.38
	Swath (km)	7.7
	VNIR MTF @ 630nm	0.23-0.27
	SWIR MTF @ 1650nm	0.28
	Spatial Co-Reg: VNIR	.18 @ Pix#126
	Spatial Co-Reg: SWIR	.21 @ Pix#131
RADIOMETRIC	Abs. Radiometry (1Sigma)	3.4%
	VNIR SNR (550-700nm)	140-190
	SWIR SNR (~1225nm)	96
	SWIR SNR (~2125nm)	38
	No. of Spectral Channels	198 Processed
SPECTRAL	VNIR (bands 8-57) (nm)	427-925
	VNIR Bandwidth (nm)	10.19-10.21
	VNIR X-trk Spec. Error (nm)	2.2
	SWIR (bands 77-224) (nm)	912-2395
	SWIR Bandwidth (nm)	10.08-10.09
	SWIR X-trk Spec. Error (nm)	0.58

Table 4: Hyperion calibrated vs. non-calibrated bands. Note the area of spectral overlap between bands 57-58 and 77-78.

VNIR channels	Band #	Wavelength (nm)	Status
	1-7	356-417nm	Not calibrated
	8-55	426-895nm	Calibrated
	56-57	913-926nm	Calibrated (overlaps with SWIR 77-78)
	58-70	936-1058nm	Not calibrated
SWIR channels	71-76	852-902nm	Not calibrated
	77-78	912-923nm	Calibrated (overlaps with VNIR 56-57)
	79-224	933-2396nm	Calibrated
	225-242	2406-2576nm	Not calibrated

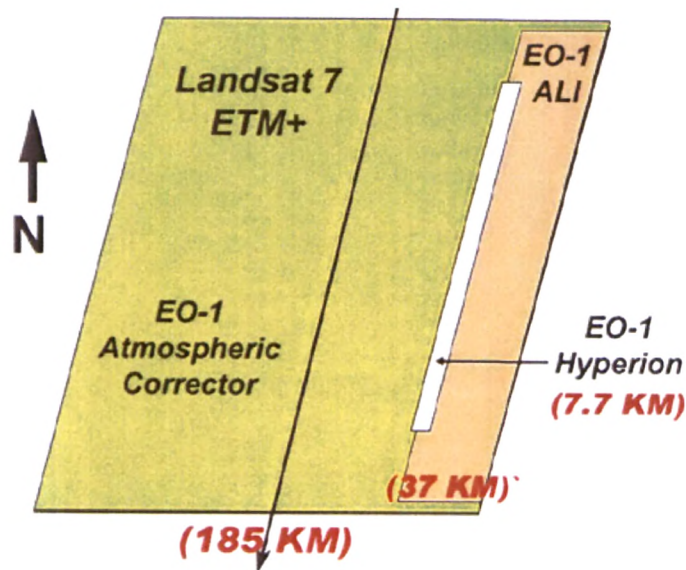Figure 10: Hyperion Sensor (Ungar et al., 2003)

Figure 11: EO-1 and Landsat-7 instrument ground tracks. The drawing traces the descending orbit ground tract with EO-1 nadir pointing
(Ungar et al., 2003)

2.3 Preprocessing of the data

The steps in the preprocessing of Hyperion data are radiometric correction, atmospheric correction, and geometric correction.

2.3.1 Hyperion Radiometric Correction

The data were delivered by USGS EROS data centre as scale radiance (Level 1 Radiometric Correction). Hyperion acquires data in pushbroom mode with two spectrometers, one in the VNIR range and another in the SWIR range. The data were scaled by 40 for the VNIR and 80 for the SWIR to convert the Level 1B1 data to units of radiance. The Hyperion sensor has higher SNR (Signal to Noise Ratio) ranging from 170-40 (VNIR – SWIR). Based on measured performance, the S/N performance was calculated (Figure 12) (Pearlman et al., 2003). Hyperion Level 1B1 data have 242 bands of which 198 are nonzero. The first 70 bands are in the VNIR in the spectral range from 356–1058 nm with an average full-width at half-maximum (FWHM) of 10.90 nm and are stored as 1.80X40XDN in W / (m² * Sr * μm). The remaining 172 bands are in the SWIR. They range from 852–2577 nm with an average FWHM of 10.14 nm and are stored as 1.18X80XDN in W / (m² * Sr * μm). A full dataset has 256 pixels and 6460 lines with the pixel size of 30 m. The

56

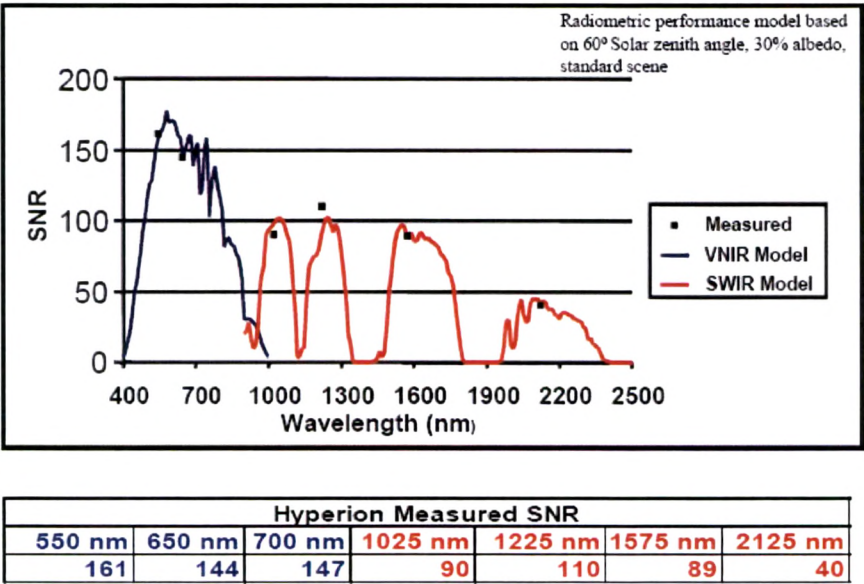data, with 12-bit quantization, is stored in HDF format as signed 16-bit integers with BIL interleaving.

Hyperion Measured SNR						
550 nm	650 nm	700 nm	1025 nm	1225 nm	1575 nm	2125 nm
161	144	147	90	110	89	40

Figure 12: Hyperion Signal-to-Noise performance (GSFC Systems Engineering Seminar, 2002)

2.3.2 Atmospheric correction

Atmospheric correction of satellite data is a major step in the retrieval of surface reflective properties. It involves removal of the effect of gaseous absorption as well as correcting for the effect of path radiance. Raw imaging spectrometer data has the general appearance of the solar irradiance curve, with radiance decreasing towards longer wavelengths, and exhibits several absorption bands due to scattering and absorption by atmospheric gases. The major atmospheric water vapor bands are centered at 940nm, 1140nm, 1380nm and 1880nm, the oxygen band at 760nm and carbon dioxide bands near 2010nm and 2080nm. The effect of atmospheric calibration algorithm is to re-scale the raw radiance data provided by imaging spectrometers to reflectance by correction for atmospheric influence thus, shifting all spectra. The result is a dataset in which each pixel can be represented by a reflectance spectrum.

Atmospheric correction is a prerequisite to most Hyperspectral Imagery (HSI) data analysis approaches. Both empirical and model-based correction methods are available. Several packages

such as ACORN (ImSpec, 2004), ATCOR (Leica, 2004) and FLAASH are commercially available for this function. FLAASH is a MODTRAN based package, less sophisticated and lesser inputs required compared with ACORN (Shih, 2004). In FLAASH with several defined atmosphere models and aerosols models, the user interface is simplified. The disadvantage of FLASSH is that it does not require the spectral center wavelength and the FWHM (Full Width Half Maximum) value. Therefore, the center wavelength shifting of each bands in Hyperion image, will not be dealt with using FLAASH which is important to remove 'smile' effects.

In this study atmospheric correction was carried out using ACORN 1.5 pb for both the data sets. Atmospheric correction was done on 196 bands after excluding non-calibrated and over-lapped 46 bands. Calibration was done for a subset of image area falling in the sanctuary which ranges from row 801-2500. A mask was generated for the Hyperion image using the band range option in ENVI (V3.6) software program (Research Systems, 2002). MNF transformation was performed to check the "spectral smile". This is similar to principal components analysis and reduces the data dimensionality in a manner that separates noise into the higher order bands. The first band typically emphasizes column-to-column issues such as a brightness gradient due to view angle, and/or variation due to cross-track smile. There is an obvious brightness gradient in MNF 1 of VNIR bands but none in MNF 1 of the SWIR bands (Goodenough et al., 2003). Figures 13 & 14 show band 1 of the MNF transform for VNIR and SWIR bands of two different data sets. In these datasets, the ACORN processing accounted for the crosstrack smile (by using mode 1.5pb), but there was a strong crosstrack gradient in the output reflectance image. The destreak processing, which normalized each column in the image removes this effect, and the MNF output in figure 15 demonstrates this with the before and after MNF band 1. Additionally a common artifact of area-array spectrometers such as Hyperion is the minor cross-track miscalibration between sensors, which manifests itself as striping in a spatial image (Asner & Heidbrecht, 2003). The destreak processing, which normalized each column in the image removes this effect, and the MNF output in figure 16 demonstrates this with the before and after MNF for band 1. Thus a "destreaking" program (Datt et al., 2003; Jupp et al., 2002) was used on Hyperion image to minimize a striping artifact present in Hyperion data.

In ACORN correction process water vapor images were generated. This calculation is made from band depth ratios at water absorption features in the original *radiance* data. This pixel by pixel water vapor value is used in the radiance to reflectance transformation in ACORN. Water vapor is estimated using the water vapor absorption bands at 940 and/or 1150 nm. A lookup table for a range of water column vapor densities is generated using MODTRAN4 and then fitted in a least-squares sense against the imaging spectrometer data. A key feature of ACORN is full spectral fitting to solve for the overlap of absorptions between water vapor and liquid water in surface vegetation.

Figures 17 & 18 show the generated water vapor images using two data sets. Standard rainbow color scheme was used for both images. Significant seasonal differences in water vapor images are apparent between the dates of April and October months. Blue color indicates low water content at the time of satellite path. Larger blue patches were observed in dry season data. More topographic variation was observed as there is lesser water vapor in the atmospheric column above areas at high elevation during dry season and more water vapor during wet season.

After atmospheric correction, resulting spectra were compared with original ones (Figures 19 & 20). Images shown in figure 19 (a, b, c) & figure 20 (a, b, c) are displayed with bands 1649nm, 854nm & 447nm as RGB and coming from two different data sets. Most striking observation about the resulting reflectance image is that there appears to be a very weak or non existent vegetation signal across the image of the dry season data. Whereas in figure 20, the resulting reflectance image appears to be a very strong vegetation signal across the image of the wet season data. This sequence of images show original radiance data, and final reflectance data for varying levels of vegetation. In figure 19 the dark green areas are those with the strongest vegetation signal, light green areas with weak vegetation signal, and the mountains south of the water body show up lighter white in this display combination and seem to have a no vegetation signal. Corresponding areas in wet season appears as dark green which are those with strongest vegetation signal across the image (Figure 20 a, b, c).
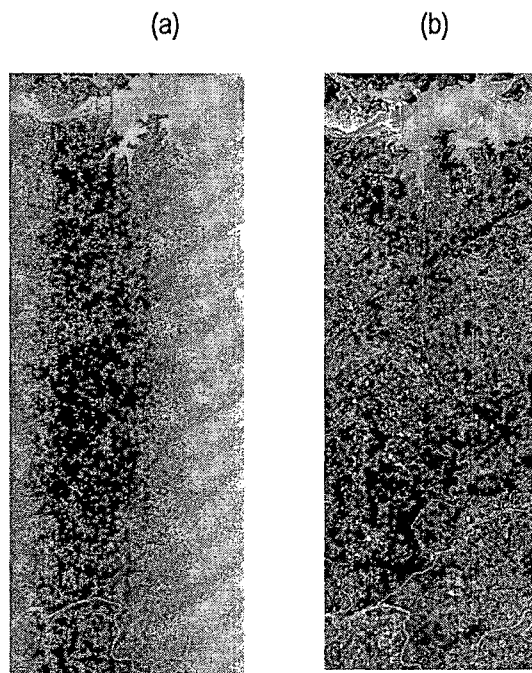
Figure 13: Brightness gradient in MNF 1 of (a) Hyperion VNIR bands and (b) SWIR bands of October month imagery
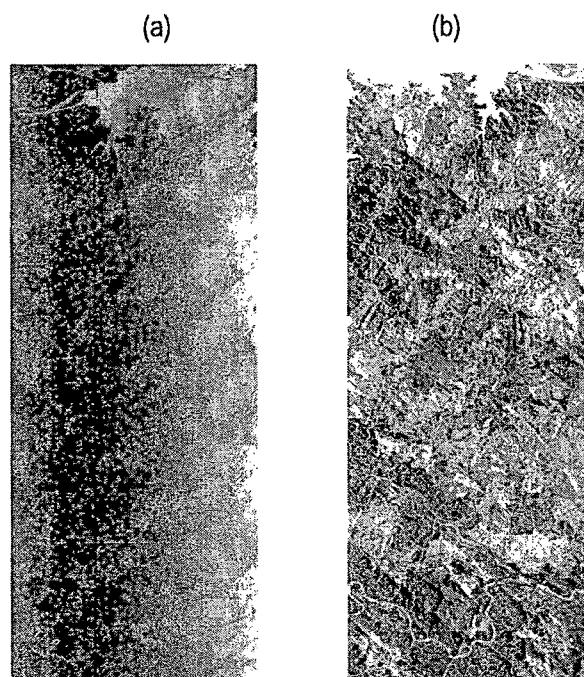

Figure 14: Brightness gradient in MNF 1 of (a) Hyperion VNIR bands and (b) SWIR bands of April month imagery
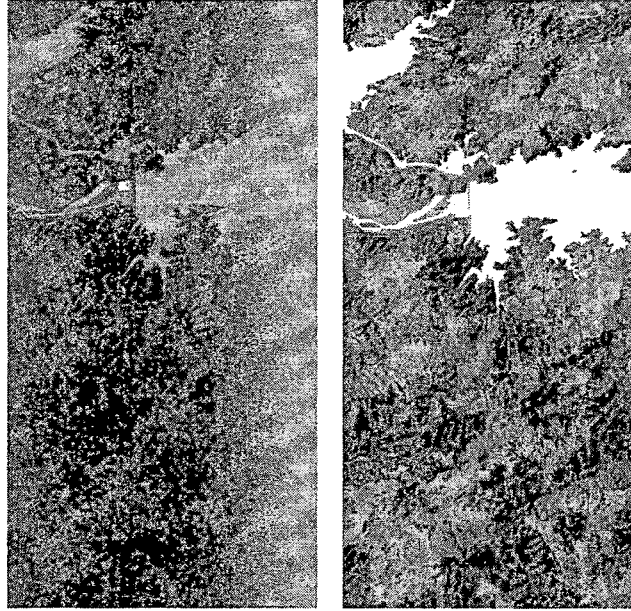
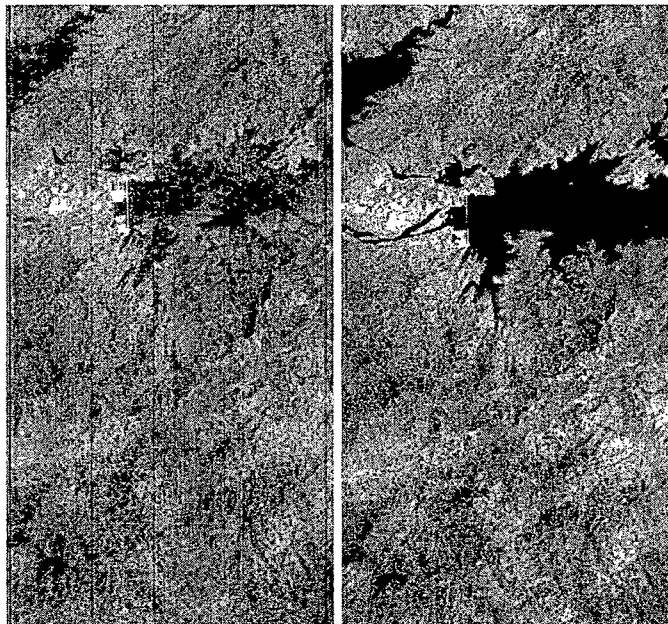Figure 15: MNF transform of VNIR bands. MNF band 1 (left) and the same after atmospheric correction (right).

Figure 16: Hyperion band at 426nm (left) and the same after removal of column striping artifact (right).
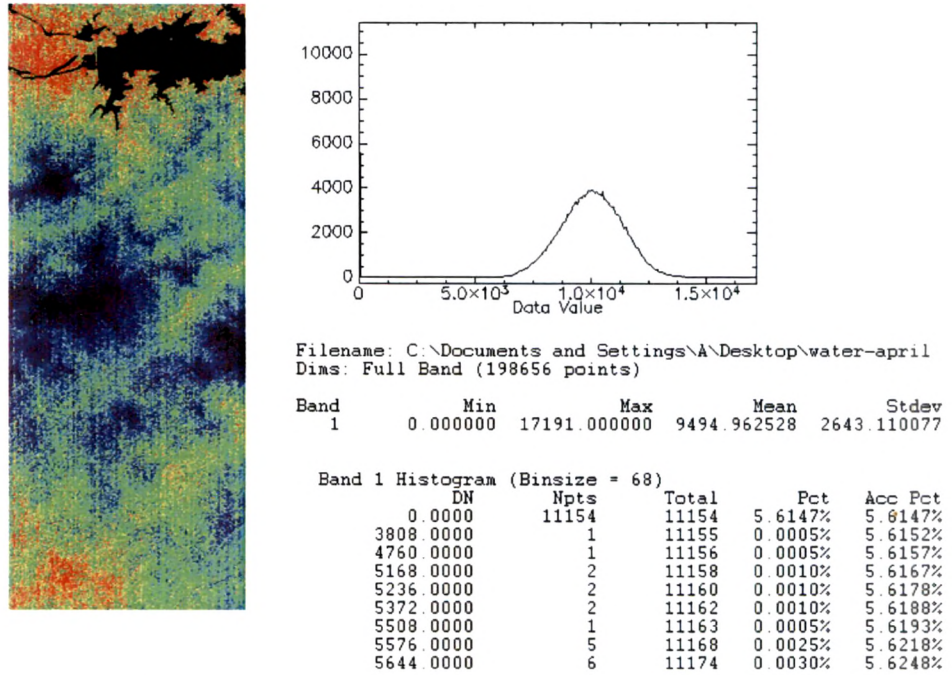
Figure 17: Water vapor image and histogram of dry season data. Precipitable water vapor (in India) in microns.
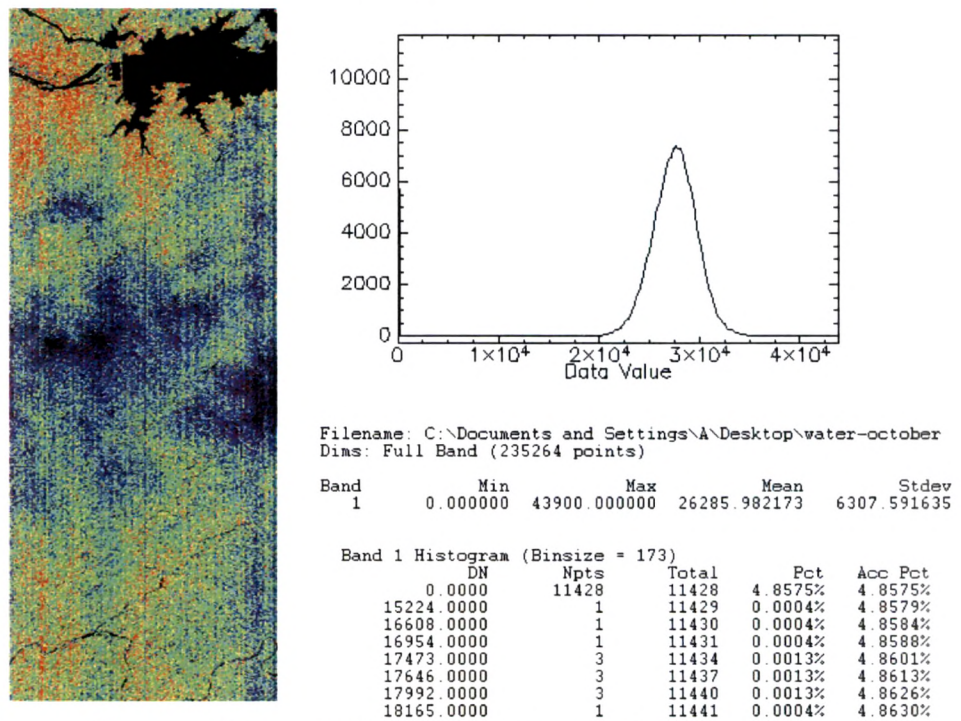

Figure 18: Water vapor image and histogram of wet season data. Precipitable water vapor (in India) in microns.
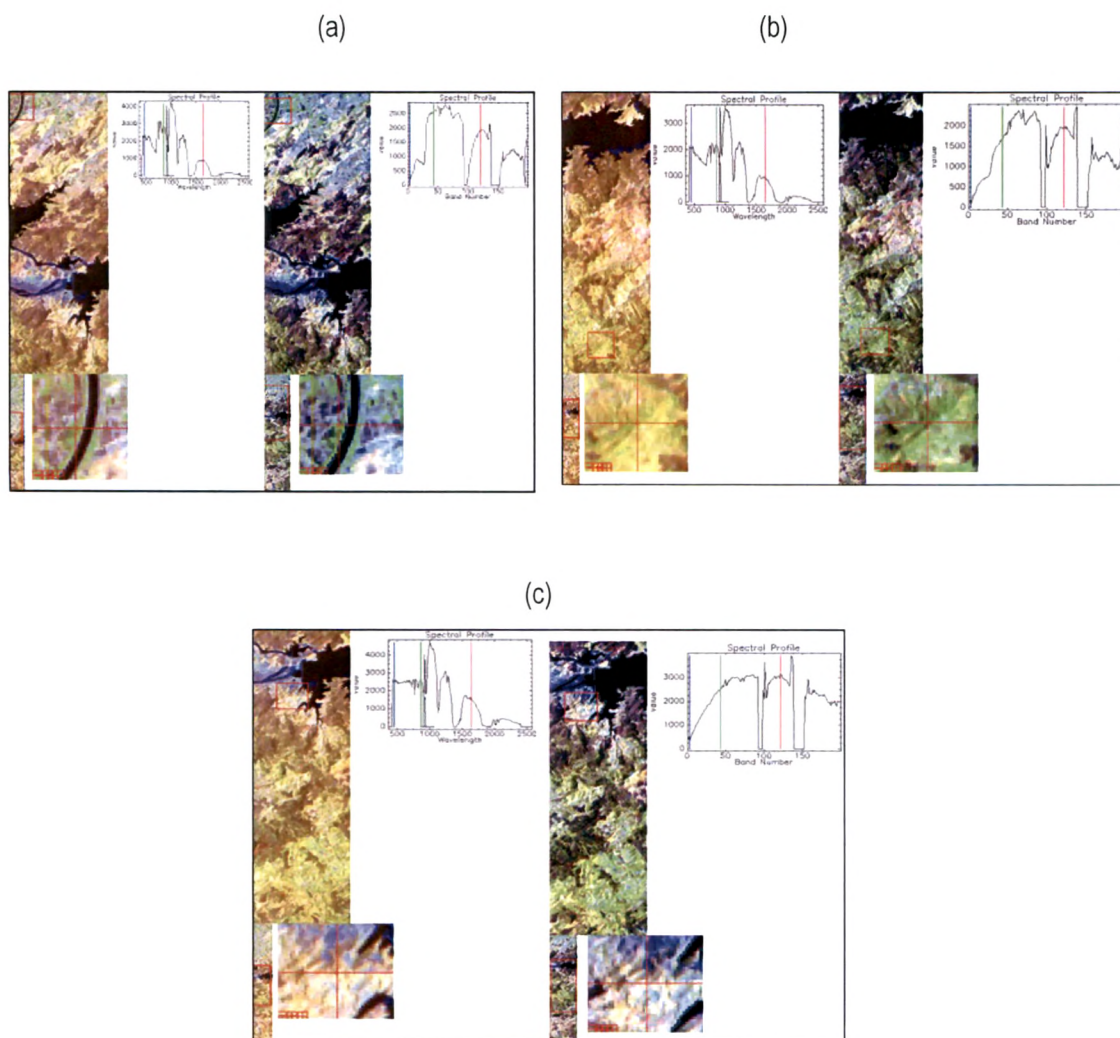
(a)　　　　　　　　　　　　　　(b)

(c)

Figure 19: Original radiance (left) and ACORN reflectance (right) extracted from dry season data. (a) A pixel with a strong vegetation signal (green peak in the visible bands). (b)A pixel with a weak vegetation signal. (c) A pixel with no vegetation signal.
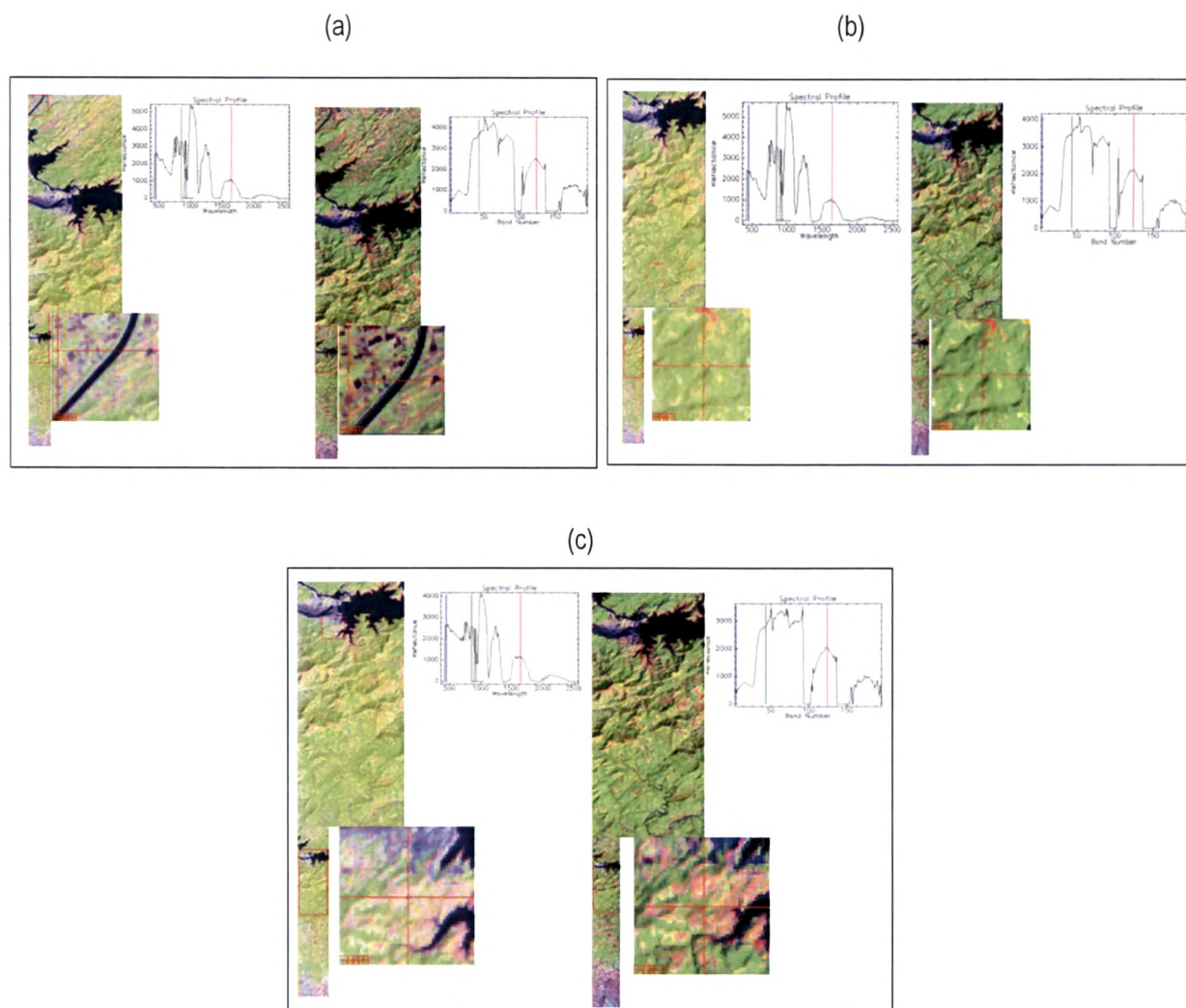
(a)

(b)

(c)

Figure 20: Original radiance (left) and ACORN reflectance (right) extracted from wet season data. (a, b, c) Pixels with a strong vegetation signal.

2.3.3 Geometric correction

Since hyperspectral imaging systems collect data pixel-by-pixel as they scan across track perpendicular to the flight line, the ground location of these pixels can jump dramatically from pixel to pixel due to the pitch, yaw and roll of the space craft's scanning instrument. Geometric correction of Hyperion imagery is therefore important for the data in order to be referenced to real world locations and to be used with other spatially referenced data sets. First ALI's (Advanced Land Imager) image (10 m Panchromatic) has been obtained at the same time and rectified to a common projection (Geographic Lat/Long & spheroid WGS 84) using 12 well identified GCPs (Ground Control Points). The resultant rectified ALI image had 0.5 pixels RMSE (Root Mean Square Error). Finally, Hyperion's atmospherically corrected subsets were geo- registered with nearest neighbour resampling to ALI's geo-registered image and resultant RMSE was 0.2 Pixels.
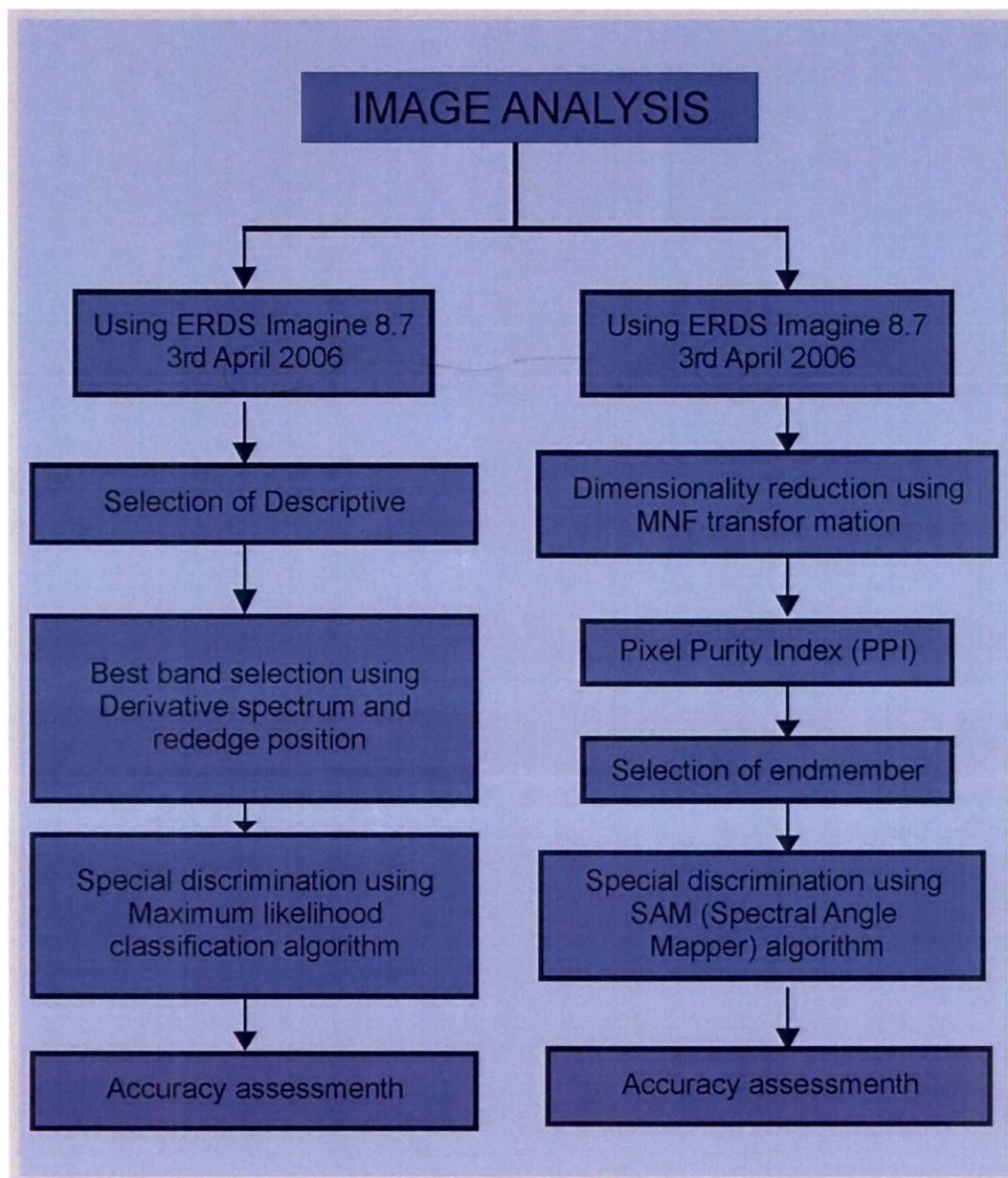
2.4. Filed Data Collection

Reconnaissance survey was done same time coinciding with data acquisition time of 3rd April, 2006 and 21st October, 2006. Field visits were made to collect information on homogenous patches, including cover type, locality, slope, and signs of disturbance. Global positioning systems (GPS) (Magellan & Leica) have been used to collect Latitude /Longitude. All these were referred as GCPs (Ground Control Points) on the Hyperion image. All the points were cross checked for accuracy. Accuracy was assessed from permanently fixed precalibrated GCPs such as bridges, river crossing, etc. Selected plot of the study area (128 sq km) was criss-crossed to locate homogenous cover of species, at least matching to the size of Hyperion pixel (30mX30m). Like in any tropical area heterogeneity in species distribution is unique to the study area. Tree species identified for analysis are given in Table 1. Excepting for *Tectona* and *Dendrocalamus* all other species showed mixed occurrence. Hence establishing an appropriate quadrat for each of the species became critical. Keeping this in mind a quadrat was selected for a species when it occupied $\geq$60% of the area. Size of each quadrat laid down was 30mX30m. Phytosociological data such as dbh (diameter breast height), height, density, and spread of canopy were recorded from each quadrat. Distance between quadrats was dependent on the type and distribution of vegetal cover, non target area. The patchiness in the distribution of tree cover was an unique feature of the study area. This was major limitation for obtaining pure spectral signatures for most of the species. For *Tectona* and

Dendrocalamus 3-4 quadrats were marked together as their distribution was relatively homogenous. Sample plots of *Tectona* and *Dendrocalamus* were selected from plantation areas to obtain pure pixel/patch and also to minimize spectral mixing of other ground objects in a single pixel of Hyperion data. For others distance between quadrats ranged from 250-500m. *Tectona* spread over a patch size of 100mX100m. *Dendrocalamus* showed coverage of 50mX80m. For others maximum occupancy as a homogenous patch was of 30mX30m. At each quadrat the tree density was inversely proportional to the value of dbh and spread of canopy. The density of *Tectona* was 75 trees with a dbh of 0.3 -0.8 m, in *Dendrocalamus* 37 clumps were with 25-80 stem density, in *Mangifera* the density was 1-7 with a dbh of 1.55-3.2m, in *Madhuca* the density was 1-5 with a dbh of 1.75-2.9m, in *Pongamia* the density was 1-2 with a dbh of 2.00-3.75m, in *Wrightia* the density was 12-15 with a dbh of 0.8-1.2m and in *Ficus* the density was 1-2 with a dbh of 5.25-6.70m. Digital photography also was made for cross verification and documentation of field status. A total of 146 quadrats were established for species level discrimination.

In forest floor study three major cover types were identified as *Tectona*, *Dendrocalamus* and other mixed dry deciduous species. Few spots of bare soil were also taken for discrimination. Selected plots were spread across an area of 112 hectares. A total of 77 observations were collected for 3 types of leaf litter cover and one of bare soil. There are 6-20 replicates for the 4 selected classes. Leaf litter thickness was recorded and distinguished as 5-10cm and 10-15cm. Thickness was measured using a scale. To look at slope variation, observations were made at two different elevations (250m & 350m). Field observations were done in the 1st and 2nd weeks of April.

2.5. Image analysis

image analysis was done based on availability of ERDS IMAGINE 8.7 and ENVI 3.6 software compatibility for Hyperspectral was also looked at. Different steps for image analysis are given below :

Flowchart of various step involved in species level discrimination using two different datasets

2.5.1. Species level discrimination using April month imagery

2.5.1.1. Descriptive spectra

Descriptive spectra for 7 tree species such as *Dendrocalamus, Mangifera, Pongamia, Ficus, Wrightia, Madhuca* and *Tectona* were evaluated from April month imagery for species level classification using ERDAS IMAGINE 8.7. Descriptive spectra for each species were developed from reference observations coming from respective number of reference quadrats laid for each species. Spectra for different girth classes of *Tectona* were also extracted. Spectra for each species were together showing clustering/bunching effect. Some of the spectra were falling away from the cluster/bunch as they were coming from quadrats where the reflectance values were influenced by background reflectance (bare soil, presence of another species, etc.). These were discarded from evaluation. A spectrum falling at the median position of the cluster was considered as a descriptive spectrum for that species. This kind of developed spectra can be compared together and the most descriptive spectrum can be selected and be considered as a pure spectrum (Lumme 2004). Descriptive spectra for all the selected species were plotted together.

2.5.1.2. Statistical analysis

2.5.1.2.1. Quantification of spectral similarity- dissimilarity

Spectral similarity – dissimilarity can be quantified using the discrimination metrics D and θ (Price 1994). For comparison, *Tectona* descriptive spectrum was used as a standard spectrum. D is a root-mean-square difference between two spectra averaged over the spectral interval of observation (400–2500nm), where

$$D = \left[\frac{1}{\lambda_b - \lambda_a} \int_{\lambda_b}^{\lambda_a} [S_M(\lambda) - S_a(\lambda)]^2 \right]^{1/2} \tag{1}$$

with S_M and S_a being the *Tectona* standard and comparison spectra, respectively, and λi the wavelength being compared. Since the sampling interval was uniform (Price 1994), the integral was replaced with a summation and computed as

68

$$D = \left[\frac{1}{N-1} \sum_{i=1}^{N} [S_M(\lambda) - S_a(\lambda)]^2 \right]^{1/2} \qquad (2)$$

with the number of spectral intervals N set equal to 168 for the dataset. The θ metric defines the shape difference between spectra and corresponds to the angle between two vectors. The spectra are normalized to remove amplitude dependence, and θ is computed as a vector dot product of the spectra using

$$\theta = \cos^{-1} \left[\frac{\int S_M(\lambda) S_a(\lambda) d\lambda}{[\int S_M(\lambda)^2 d\lambda]^{1/2} [\int S_a(\lambda)^2 d\lambda]^{1/2}} \right] \qquad (3)$$

where S_M and S_a again correspond to the *Tectona* standard and the comparison spectra at each wavelength λ.

2.5.1.2.2. Test of Significance

ANOVA were carried out to observe that the differences seen are significant ($\alpha=.01$) amongst descriptive spectra of 7 different tree species with respect to phenology and the difference amongst reflectance spectra of different girth class for *Tectona*.

2.5.1.3. Derivative spectra for the selection of best bands

Derivatives of spectra are commonly employed in hyperspectral investigations of vegetation (Castro-Esau et al., 2004; Van Aardt & Wynne, 2001; Cochrane, 2000). Derivatives are relatively less sensitive to variations in illumination intensity caused by cloud cover and topography (Tsai & Philpot, 1998) and hence should enhance the spectral contrast between different classes. It is suggested that spectral derivatives have important advantages over spectral reflectance, such as their ability to reduce variability due to changes in illumination or background reflectance (Curran et al., 1991). Many workers used derivatives to define the position of the red edge (λ_{RE}) (Lichtenthaler et al., 1999; Jago et al., 1999). First derivative indicates the change in velocity and the second derivative indicates change in acceleration. In this study the first derivative spectra were computed

using the first order difference, which is an approximation of the differential in each spectral channel (1).

$$dRsi/dW = (Rs_{i+1} - Rs_{i-1}) / (W_{i+1} - W_{i-1}) \tag{4}$$

where Wi is the wavelength of channel i in nanometers and Rsi is the reflectance in ith channel (Danson et al., 1992).

First derivative spectra display the variation with wavelength in the slope of the original reflectance spectrum. Here first derivative was used to select best bands for species level discrimination. The three bands selected for classification came from red edge region (701nm) and from SWIR regions (1386nm, 1739nm).

2.5.1.4. The Red-edge position

The red edge is an unique feature of green vegetation. Within this red edge region the point of maximum slope is referred to red edge position (Filella & Peñuelas, 1994). Typically it occurs between 670 – 780 nm. Although it is principally sensitive to chlorophyll, the red edge has been shown sensitive also to water, foliage mass and leaf area index (LAI) (Curran et al., 1991; Danson and Plummer, 1995; Dawson and Curran, 1998). In this study the red-edge position was calculated for all selected species using linear-four point interpolation method (Guyot & Baret, 1988).

2.5.1.4.1. Linear four-point interpolation technique

The linear four-point interpolation method (Guyot & Baret, 1988) assumes that the reflectance curve at the red edge can be simplified to a straight line centered near the midpoint between the reflectance in the near infra-red (NIR) at about 780 nm and the reflectance minimum of the chlorophyll absorption feature at about 670 nm. It uses four wavebands (670, 700, 740 and 780 nm), and the REP is determined by using a two step calculation procedure

Calculation of the reflectance at the inflection point

$$R_{re} = (R_{670} + R_{780})/2 \tag{5}$$

Where, R is the reflectance.

Calculation of the red edge wavelength or red edge position is according to Eq. 6

$$REP = 700 + 40 \left(\frac{R_{re} - R_{700}}{R_{740} - R_{700}} \right)$$

(6)

where, 700 and 40 are constants resulting from interpolation in the 700–740 nm interval.

2.5.1.5. Species level discrimination

7 Tree species identified for discrimination are given in Table 1. Three Hyperion bands selected were used for these 7 tree species discrimination. An attempt was made to classify *Tectona* (Teak) into two girth classes: 18-60cm (Teak young) & 90-260cm (Teak old). Excluding the selected species, all other land cover types such as agricultural land, barren land, human settlement, etc. were considered in a single class as "Others" in classification. A total of 9 classes were selected. A supervised classification was done in which spatially discrete pixels of each of the 9 selected classes were used to extract spectral signatures for each class (49 reference observations). The remaining 56 field observations (of the total 105 observations) were used in accuracy assessment as independent samples. A maximum likelihood classification was used to assign all pixels in the image into one of the 9 signature classes using the 3 sensitive bands. Specific probability values were used to assign all pixels in the subset into one of the 9 signature classes (Σp=1). Probability values of occupancy to each signature class have been given based on field observations. The statistical probability that a given pixel belongs to a particular class is computed by maximum likelihood algorithm.

The **maximum likelihood** algorithm assumes that the histograms of the bands of data have normal distributions. The maximum likelihood decision rule is based on the probability that a pixel belongs to a particular class. The basic equation assumes that these probabilities are equal for all classes, and that the input bands have normal distributions (ERDAS user guide).
The equation for the maximum likelihood is as follows:

$$D = \ln(a_c) - [0.5 \ln(|Cov_c|)] - [0.5 (X-M_c)^T (Cov_c^{-1}) (X-M_c)]$$

(7)

Where:

D =   weighted distance (likelihood)

71

C	=	a particular class
X	=	the measurement vector of the candidate pixel
M_c	=	the mean vector of the sample of class c
a_c	=	percent probability that any candidate pixel is a member of class c
		(defaults to 1.0, or is entered from *a priori* knowledge)
Cov_c	=	the covariance matrix of the pixels in the sample of class c
$|Cov_c|$	=	determinant of Cov_c (matrix algebra)
Cov_c-1	=	inverse of Cov_c (matrix algebra)
ln	=	natural logarithm function
T	=	transposition function (matrix algebra)

2.5.1.6. Accuracy assessment

Two measures of classification accuracy, overall accuracy assessment (OAA) & kappa coefficient have been calculated (Buddenbaum et al., 2005, Congalton, 1991). Overall accuracy (OAA) quantifies the percentage of cases correctly classified:

$$OAA = \frac{1}{n}\sum_{1}^{q} n_{kk} * 100$$

(8)

where n_{kk} is the number of correctly classified validation pixels (confusion matrix diagonals), q is the number of classes, and n is the total number of validation pixels used. Producer's accuracy was calculated by dividing the number of pixels correctly classified for each class by the total number of training pixels for that class, while user's accuracy was the number of correctly classified pixels divided by the total number of classified pixels for that class. Finally, the kappa coefficient was calculated as a measure of the significance of the classification results relative to chance agreement.

$$KAPPA = \frac{n\sum_{k=1}^{q} n_{kk} - \sum_{k=1}^{q} n_{k+}n_{+k}}{n^2 - \sum_{k=1}^{q} n_{k+}n_{+k}}$$

(9)

where n_{k+} is the sum of the validation pixels in a class and n_{+k} is the sum of the classified pixels in that class. A kappa value of zero indicates that a classification is no better than random assignment of pixels, while a value of one indicates perfect agreement between training pixels and their prescribed classes (Lillesand & Kiefer, 2000).

2.5.2. Species level discrimination using October month imagery
Below given steps were performed using ENVI 3.6 software.

2.5.2.1. Minimum Noise Fraction (MNF) Transformation

The minimum noise fraction (MNF) transformation is used to determine the inherent dimensionality of image data, to segregate noise in the data, and to reduce the computational requirements for subsequent processing (Boardman & Kruse, 1994). This step is often completed as a precursor to other types of analysis. Basically it is a way of simplifying the data. The MNF transform is essentially two principal component transformations. The first transformation, based on an estimated noise covariance matrix, decorrelates and rescales the noise-in the data. This first step results in transformed data in which the noise has unit variance and no band-to-band correlations. The second step is a standard principal components transformation which creates several new bands containing the majority of the information. For the purposes of further spectral processing, the inherent dimensionality of the data is determined by examination of the final eigenvalues and the associated images. The data space can be divided in to two parts: one part associated with large eigenvalues and coherent eigenimages, and a complementary part with near-unity eigenvalues and noise-dominated images. By using only the coherent portions, the noise is separated from the data, thus improving spectral processing results. The image pixels are presented by eigenvalues. For the purpose of further spectral processing, the dimensionality of the data is determined by examination of these values.

MNF transformation was performed on all 165 bands, after excluding bands whose signal was significantly diminished by atmospheric absorption of water, ozone, CO_2 and other gases (Clark, 1999). In examining the eigenvalues, it can be seen that the first 15 MNF bands have large eigenvalues (11.20 to 2.38 SNR). The remaining low value bands are seen as noise. The images

show the information compressed into only a few bands. Therefore, the redundancy of the data is eliminated and noise is also removed.

2.5.2.2. Pixel Purity Index (PPI)

All remotely sensed images contain a phenomenon known as mixed pixels. These are the pixels that contain a mix of features. In hyperspectral analysis it is useful to separate purer from more mixed pixels in order to reduce the number of pixels to be analyzed for endmember separation and identification. The pixel purity index is a way of finding the most spectrally pure pixels in images (Boardman, 1993; Boardman et al., 1995; ENVI, 2002). The PPI stipulates how many times the pixel is extreme in the simplex (Boardman & Kruse, 1994; Boardman et al., 1995). The most spectrally pure pixels typically correspond to the number of times that this pixel was recorded as extreme. This way, threshold of the PPI image can stipulate the most extreme pixels results in further spatial reduction.

PPI was performed on selected MNF bands. Different MNF band combinations were selected such as 1-2, 1-3 up to 1-15 to extract purest pixels for each species. PPI was confirmed by 10,000 iterations. Each MNF band combination has given different number of pure pixels. Field observations were overlaid for each species. Number of purest pixels and hits for each species were observed and data value/number of iterations (the number of times that pixel was recorded as an extreme) of each of these pixels were recorded. Band combination was different for different species. For example, higher number of hits for *Tectona* and *Dendrocalamus* were found in 1-5 MNF band combination. While for others it was in 1-10 MNF band combination. Hence, 1-5 MNF band combination was used as an unique band combination to select correct endmember of *Tectona* and *Dendrocalamus* for subsequent analysis. For other species, 1-10 band combination was used to select endmember spectra.

2.5.2.3. Endmember selection

Endmember spectra for each species were selected manually from the developed PPI image. Field observations were overlaid for each species. Numbers of iterations of GCP locations of each species were extracted. Pixel locations having maximum number of iterations were considered as endmember for respective species. Spectra of these pixels were used as library spectra of selected

74

tree species for further analysis. Five endmembers were selected for *Tectona, Dendrocalamus, Mangifera, Madhuca* and *Ficus.*

2.5.2.4. Spectral Angle Mapper (SAM)

The Spectral Angle Mapper (SAM) is a physically-based spectral classification that uses an *n*-dimensional angle to match pixels to reference spectra. The algorithm determines the spectral similarity between two spectra by calculating the angle between the spectra, treating them as vectors in a space with dimensionality equal to the number of bands (Kruse et al., 1993; Price, 1994). This technique, when used on calibrated reflectance data, is relatively insensitive to illumination and albedo effects. Endmember spectra used by SAM can come from ASCII files, spectral libraries, or can be extracted directly from the image (as ROI average spectra). SAM compares the angle between the endmember spectrum vector and each pixel vector in *n*-dimensional space. Smaller angles represent closer matches to the reference spectrum. Pixels further away than the specified maximum angle threshold in radians are not classified.

$$\alpha = \cos^{-1}\left(\frac{\sum_{i=1}^{nb} t_i r_i}{\left(\sum_{i=1}^{nb} t_i^2\right)^{1/2}\left(\sum_{i=1}^{nb} r_i^2\right)^{1/2}}\right) \qquad (10)$$

Where *nb* = the number of bands

ti = test spectrum

ri = reference spectrum

In general, pixels belonging to the same class have small spectral angle, and spectral angles of pixels of different types are large. Five tree species identified for discrimination are given in Table 1. SAM was performed using the selected endmembers of each species as different classes. To minimize false detection in this study no threshold value was used in classification. It was performed for the entire spectrum (all 196bands), VIS+NIR region (1-90bands), SWIR-I region (103-136bands), SWIR-II region (159-195bands), 1-10 MNF and 1-15 MNF bands.

2.5.2.6. Accuracy assessment

141 hits (of the total 146 observations) from collected GCP's of five tropical tree species were used for accuracy assessment. Two measures of classification accuracy (User's and Producer's accuracy), overall accuracy assessment (OAA) & KAPPA coefficient were calculated (Buddenbaum et al., 2005, Congalton 1991).

2.5.3. Forest floor cover studies

2.5.3.1. Descriptive spectra

Descriptive spectra were evaluated for dry deciduous forest floor cover studies. Descriptive spectra for 4 cover types (*Tectona, Dendrocalamus*, mixed deciduous species and bare soil) were extracted from 3-9 observations. Spectra for each cover type were together showing clustering/bunching effect. Some of the spectra were falling away from the cluster/bunch as the reflectance values of few observations were influenced by background noise (such as presence of other woody material). These were discarded from analysis. A spectrum falling at the median position of the cluster was considered as a descriptive spectrum for that cover type. They were distinct from each other. Descriptive spectra were developed for different cover types with similar or different thickness of litter. Altitude variation has also been looked into.

2.5.3.2. Continuum removal spectra

In order to compare the shapes of the absorption features Kokaly (2001) used a method of normalization called continuum removal. Continuum removal or base line normalization is a method commonly used in laboratory infrared spectroscopy (Ingle, 1988). The continuum removal method allows one to compare absorption features from a common baseline (Lee et al., 2005). This technique was employed to discriminate the 4 cover types as they are playing major role in dry deciduous forest floor cover. Continuum removed spectra were developed using ENVI 3.6 software.

2.5.3.3. Discrimination of cover types

Effort was made to discriminate 4 major cover types (*Tectona, Dendrocalamus*, mixed deciduous species and bare soil) using dry season (April month) data. To discriminate these 4 cover types

specific bands were selected using continuum removal spectra. Two regions with maximum separation were identified. Selected bands (690nm, 2113nm & 2234nm) were coming from VIS & SWIR-II regions of the spectrum. Maximum likelihood classification was performed. Accuracy assessment report also was developed.